AGU ADVANCING EARTH AND SPACE SCIENCES

Geophysical Research Letters

RESEARCH LETTER
10.1029/2023GL105919

Disentangling the Advective Brewer-Dobson Circulation Change

P. Šácha[1], R. Zajíček[1,2], A. Kuchař[3], R. Eichinger[1,4], P. Pišoft[1], and H. E. Rieder[3]

[1]Department of Atmospheric Physics, Faculty of Mathematics and Physics, Charles University, Praha, Czech Republic, [2]Institute of Atmospheric Physics CAS, Prague, Czech Republic, [3]Institute of Meteorology and Climatology, University of Natural Resources and Life Sciences, Vienna (BOKU), Vienna, Austria, [4]Deutsches Zentrum für Luft- und Raumfahrt (DLR), Institut für Physik der Atmosphäre, Weßling, Germany

Key Points:

- A method for attributing net upwelling trends to changes in circulation, air density and structure of the upwelling region is established
- Models agree largely on contributions from vertical shifts in pressure surfaces/tropopause and changes in vertical advection
- For reanalyses, on the other hand, the uncertainty is larger, not allowing direct constraints on model trends

Supporting Information:

Supporting Information may be found in the online version of this article.

Correspondence to:

P. Šácha,
petr.sacha@matfyz.cuni.cz

Citation:

Šácha, P., Zajíček, R., Kuchař, A., Eichinger, R., Pišoft, P., & Rieder, H. E. (2024). Disentangling the advective Brewer-Dobson circulation change. *Geophysical Research Letters*, *51*, e2023GL105919. https://doi.org/10.1029/2023GL105919

Received 15 AUG 2023
Accepted 13 MAY 2024

Author Contributions:

Conceptualization: P. Šácha, H. E. Rieder
Data curation: R. Zajíček, A. Kuchař, R. Eichinger, P. Pišoft
Formal analysis: R. Zajíček, A. Kuchař
Funding acquisition: P. Šácha, P. Pišoft
Investigation: P. Šácha, R. Zajíček, A. Kuchař
Methodology: P. Šácha, R. Zajíček
Project administration: P. Šácha, P. Pišoft
Resources: R. Zajíček, A. Kuchař
Software: R. Zajíček, A. Kuchař
Supervision: P. Šácha, H. E. Rieder
Validation: R. Zajíček, A. Kuchař
Visualization: R. Zajíček, A. Kuchař, R. Eichinger, P. Pišoft

Abstract Climate models robustly project acceleration of the Brewer-Dobson circulation (BDC) in response to climate change. However, the BDC trends simulated by comprehensive models are poorly constrained by observations, which cannot even determine the sign of potential trends. Additionally, the changing structure of the troposphere and stratosphere has received increasing attention in recent years. The extent to which vertical shifts of the circulation are driving the acceleration is under debate. In this study, we present a novel method that enables the attribution of advective BDC changes to structural changes of the circulation and of the stratosphere itself. Using this method allows studying the advective BDC trends in unprecedented detail and sheds new light into discrepancies between different data sets (reanalyses and models) at the tropopause and in the lower stratosphere. Our findings provide insights into the reliability of model projections of BDC changes and offer new possibilities for observational constraints.

Plain Language Summary The large-scale interhemispheric meridional overturning circulation in the middle atmosphere determines the composition of this region, including the distribution of radiatively important trace gases. The long-term change of this circulation is a subject of ongoing debate, and an area of disagreement between models and observations. In our study we present a method that provides an unprecedented insight into the change and disentangles the individual factors behind it. Hence, the method introduces new constraints on the circulation change and can aid the reconciliation between models and observations.

1. Introduction

Changes in atmospheric composition since pre-industrial times have warmed surface climate (IPCC, 2022), altered the atmospheric structure (Pisoft et al., 2021; Santer et al., 2003), temperature (Maycock et al., 2018; Santer et al., 2023), and affected the dynamics (Shepherd & McLandress, 2011) and transport (Garcia & Randel, 2008) of the stratosphere. In turn, the chemical makeup of the middle atmosphere (Andrews et al., 1987), including the distribution and trends of radiatively important gases such as ozone ("Scientific assessment of ozone depletion: Executive Summary, 2022", 2022) and water vapor (Solomon et al., 2010), is dynamically governed by the Brewer-Dobson circulation (BDC), the large-scale interhemispheric meridional overturning circulation (Plumb, 2002). The BDC is commonly defined (Butchart, 2014) as consisting of a diffusive and an advective part, the latter described by the residual mean circulation (Eichinger et al., 2019). In studies investigating BDC changes, a frequently explored proxy for the advective BDC component is the net tropical upwelling across the 70 hPa (Butchart et al., 2010) or 100 hPa (Abalos et al., 2021) isobars or the tropopause (Ortland & Alexander, 2014), which quantifies the amount of mass advected by the residual mean circulation from the troposphere into the stratosphere and beyond.

Given the importance of the BDC for atmospheric composition, a realistic representation of the structure, strength, and variability of the circulation remains crucial for earth system and chemistry-climate modeling (Abalos et al., 2021). Comprehensive global climate models unanimously indicate a strengthening of BDC, including its advective part, in recent decades, which is projected to continue and amplify with progressing climate change. Key drivers of the trend are not only the changes in CO_2 and CH_4 abundances but also ozone depleting substances (Muthers et al., 2016; Polvani et al., 2018). This acceleration dominates the projected middle atmosphere changes throughout the 21st century (Butchart, 2014). However, recent BDC trends diagnosed from model fields do not match observations regarding the sign of the trend (Davis et al., 2023; Stiller et al., 2017) and

Writing – original draft: P. Šácha, H. E. Rieder
Writing – review & editing: P. Šácha, R. Zajíček, A. Kuchař, R. Eichinger, P. Pišoft, H. E. Rieder

there is also a significant intermodel spread in the magnitude of recent and future trends (Abalos et al., 2021; Butchart et al., 2010; Hardiman et al., 2014).

Another robust impact of changes in atmospheric composition is the changing vertical structure of the atmosphere. While the troposphere is warming and thermally expanding (Santer et al., 2003; Vallis et al., 2014), the stratosphere is cooling and contracting (Pisoft et al., 2021). It has been shown that these changes in atmospheric vertical structure interfere with the diagnosed BDC trends (Eichinger & Šácha, 2020; Shepherd & McLandress, 2011; Šácha et al., 2019). Among others it has been illustrated that no robust increase can be detected in the net tropical upwelling when heuristically accounting for the tropopause rise (Oberländer-Hayn et al., 2016). Besides this, the horizontal structure of the tropospheric (Staten et al., 2020) and stratospheric (Fu & Lin, 2011) circulation is also changing, which might affect BDC trends (Stiller et al., 2017) and thus make causal attribution of potential BDC trends an even trickier task. Moreover, there is a documented spread between climate models in the vertical (Eichinger & Šácha, 2020) and horizontal (Hardiman et al., 2014) structure of the upwelling region.

In this paper we study to what extent these structural changes contribute to simulated trends of the advective BDC for individual models. Consequently, comparing the models with reanalyses, we want to understand whether the differences between model and reanalysis trends of the advective BDC component can be caused by a different mixture of circulation increase and vertical and horizontal structure change rates. Unraveling the role of structural changes for the BDC change, and quantifying their contribution, could aid reconciling the disagreement between observations and models regarding BDC trends in the (recent) past (WMO, 2018) and enhance confidence in future projections of BDC changes by global chemistry-climate (CCMs) and earth system models (ESMs).

The paper is structured as follows. First we derive the method for decomposition of the BDC changes and describe the statistical approach and data sets. Then we demonstrate the utility of the method by applying it to state-of-the-art ESM simulations of the recent past, trying to constrain the model results with multi-reanalysis mean. The results section ends with an analysis of differences between individual reanalyses. The paper concludes with a summary of the results, a discussion on the projections of future advective BDC changes and their uncertainty and an outlook of how the method can be further expanded to provide additional constraints for models from observations.

2. Methods and Data

The cornerstone of this study is the formulation and application of a method that allows separating and quantifying the role of the accelerating flow velocity, structural changes and density variations behind the advective BDC interannual changes. The basic idea is to reconstruct the upwelling changes diagnosed on a time-variable level (isobars, the tropopause etc.) into contributions from these mechanisms evaluated in the geometric height (z-) coordinate, as depicted in Figure 1.

For studying the long-term changes in BDC strength, it is in this respect advantageous to define a single scalar indicator, either the net upwelling or downwelling mass flux across a specified level. Here, we are concerned with the net upwelling across traditionally used pressure levels (100 and 70 hPa) and across the tropopause. The zonal mean tropopause (TPP) and also the zonal mean isobars define parameterized curves in the z, φ (latitude) plane with a time-variable location and shape, $\overline{z}(t,\varphi)$. The advective zonal mean mass transport M across an oriented element of the zonal mean curve, represented by a vector $\overrightarrow{\mathrm{d}l}(\overline{z}(t,\varphi),t,\varphi)$, is given as:

$$\mathrm{d}M(\overline{z}(t,\varphi),t,\varphi) = 2\pi a \cos\varphi\, \overline{\rho}(\overline{v}^*,\overline{w}^*)\cdot\overrightarrow{n}\,\mathrm{d}l, \tag{1}$$

where a is the radius of the Earth, $\overline{\rho} = \overline{\rho}(\overline{z}(t,\varphi),t,\varphi)$ is the zonal mean density at the respective level (itself a function of time t and latitude φ), $\overline{w}^* = \overline{w}^*(\overline{z}(t,\varphi),t,\varphi)$ and $\overline{v}^* = \overline{v}^*(\overline{z}(t,\varphi),t,\varphi)$ are the vertical and meridional residual mean velocity components evaluated at the respective zonal mean levels, $\overrightarrow{n}(\overline{z}(t,\varphi),t,\varphi)$ is a normal vector of the oriented element of the zonal mean curve and $\mathrm{d}l(\overline{z}(t,\varphi),t,\varphi)$ is the length of the zonal mean curve element. Note that the location, length and shape (quantified by the angle α it makes with the horizontal) of the zonal mean curves vary with time.

The net zonal mean advective mass transport across the selected level is then computed as an integral of $\mathrm{d}M$ from the South to the North pole along the curve. Concentrating only on the part of the advective mass transport from

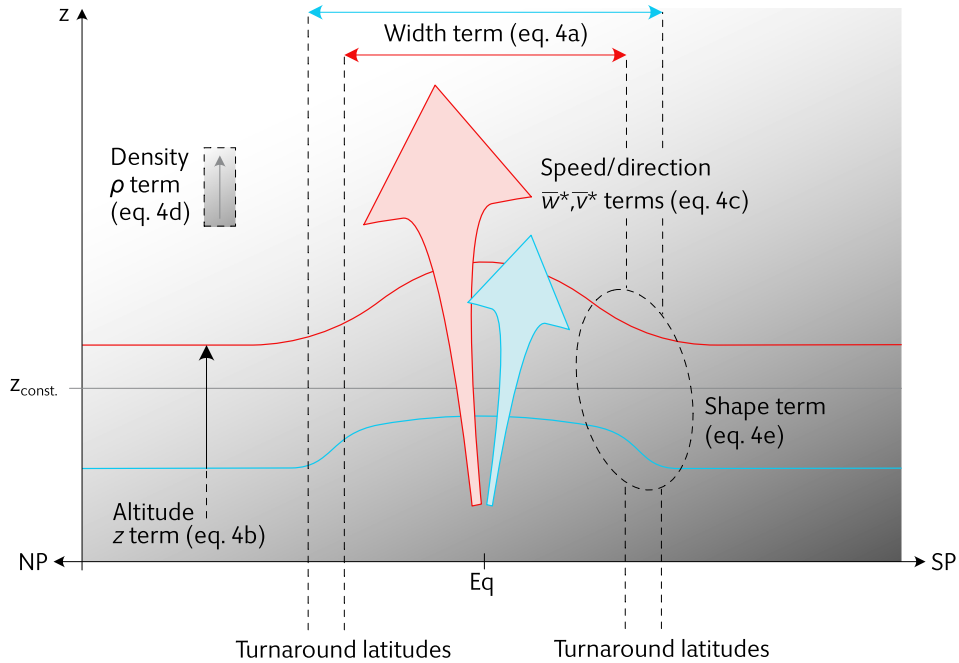

Figure 1. Schematic illustration of the contributions to the change of the net upwelling across a level that changed its location and geometry in the geometric height vertical coordinate system between the time instant A (blue line) and B (red line). The net change consists of contributions from changes of the speed (size of the arrow) and direction (inclination of the arrow) of the circulation, from changing density of air (shading, also subject to vertical shift), from changes in the width of the upwelling region, from the vertical shift (height changes) of the level and changes in the shape of the zonal mean curve drawn by the selected level controlling the effectivity of the meridional transport.

lower to upper levels, we diagnose first the time varying boundaries between the upwelling and downwelling regions (φ_1, φ_2) as latitudes where the zonal mean advective transport across the level changes sign. Then, we compute the net upwelling (U) across the selected level evaluated by following the time variable curve L in the geopotential height vertical coordinate system as:

$$U(L,t) = \int_{\varphi_1(t)}^{\varphi_2(t)} \mathrm{d}\, M(\overline{z}(L,t,\varphi),t,\varphi). \tag{2}$$

After having computed the annual-mean time-series of upwelling according to this definition, we are ready to derive the kinematic factors contributing to its year-to-year change δU, defined as:

$$\delta U = U(L,t+\delta t) - U(L,t). \tag{3}$$

Differentiating the integral (Equation 2), using the Leibniz integral rule, invoking an analogy to the material derivative concept and after some manipulations (for the complete derivation please refer to the Text S1 in Supporting Information S1), we obtain on the first order of δt a complete decomposition of the net upwelling change across any continuous zonal mean curve in the form:

$$\delta U = \overbrace{\int_{\varphi_2(t)}^{\varphi_2(t+\delta t)} \mathrm{d}\, M(\overline{z}(t^*,\varphi),t^*,\varphi) - \int_{\varphi_1(t)}^{\varphi_1(t+\delta t)} \mathrm{d}\, M(\overline{z}(t^*,\varphi),t^*,\varphi)}^{\text{width term}} + \tag{4a}$$

$$+\overbrace{2\pi a^2 \int_{\varphi_1}^{\varphi_2} \frac{\partial \overline{z}}{\partial t} \frac{\partial \overline{\rho}(\overline{w}^* + \overline{v}^* \tan\alpha)}{\partial z} \cos\varphi \,\mathrm{d}\varphi}^{\text{z term}} \cdot \delta t + \tag{4b}$$

$$\overbrace{+2\pi a^2 \int_{\varphi_1}^{\varphi_2} \overline{\rho} \frac{\partial \overline{w}^*}{\partial t} \cos\varphi \, d\varphi \cdot \delta t}^{\overline{w}^* \text{term}} \overbrace{+2\pi a^2 \int_{\varphi_1}^{\varphi_2} \tan\alpha \overline{\rho} \frac{\partial \overline{v}^*}{\partial t} \cos\varphi \, d\varphi \cdot \delta t}^{\overline{v}^* \text{term}} + \quad (4c)$$

$$\overbrace{+2\pi a^2 \int_{\varphi_1}^{\varphi_2} \overline{w}^* \frac{\partial \overline{\rho}}{\partial t} \cos\varphi \, d\varphi \cdot \delta t + 2\pi a^2 \int_{\varphi_1}^{\varphi_2} \tan\alpha \overline{v}^* \frac{\partial \overline{\rho}}{\partial t} \cos\varphi \, d\varphi \cdot \delta t}^{\rho \text{term}} + \quad (4d)$$

$$\overbrace{+2\pi a^2 \int_{\varphi_1}^{\varphi_2} \frac{\overline{\rho} \overline{v}^*}{\cos^2\alpha} \frac{\partial \alpha}{\partial t} \cos\varphi \, d\varphi \cdot \delta t}^{\text{shape term}} . \quad (4e)$$

The decomposition (Equation 4) reveals a complete set of mechanisms contributing to changes of the net upwelling following a selected level as viewed in the z-system. These are the change in the width of the upwelling region (width term), the vertical shift of the level (z term), the contributions from the local accelerations of the vertical ($\overline{w}^*$ term) and meridional ($\overline{v}^*$ term) components of the residual mean velocity, the contribution from the local density change (ρ term), and finally the contribution from the change in the local zonal mean curve inclination (shape term).

In Figure 1, we illustrate schematically, how these mechanisms contribute to the net upwelling changes. While the speed and direction of the residual mean circulation, the vertical shift of the respective level, and density of air at a specific level have been considered in isolation or (partial) combination in previous studies, our study breaks new ground by proposing a consistent framework also considering the changes in geometrical features of the upwelling region. Furthermore, the presented method allows to decompose the upwelling or downwelling across any other level (e.g., isentropic levels). Although the net upwelling and downwelling changes must be approximately equal, the relative importance of individual mechanisms revealed by the decomposition may differ.

To make the methodology more accessible, we hereafter present three illustrative, theoretical cases of upwelling changes. In all of these, we assume that the width of the upwelling region, geometry of the surface and $\overline{v}^*$ remain constant. In the first example, we assume that also $\overline{w}^*$ and density, and hence the net upwelling remain constant in height. If the pressure levels are rising, the net upwelling diagnosed on pressure levels (the left hand side of Equation 4) will decrease, due to the exponential decrease of the mass flux with height. From the decomposition, the width, shape, density, $\overline{v}^*$ and $\overline{w}^*$ terms are zero from assumptions on their local tendencies. Hence, only the z term will be strongly negative as $\frac{\partial \overline{z}}{\partial t}$ is positive and $\frac{\partial \overline{\rho}(\overline{w}^* + \overline{v}^* \tan\alpha)}{\partial z}$ is negative. Note that for this hypothetical example to be plausible and $\frac{\partial \overline{\rho}}{\partial t}$ to be zero, one has to assume a local positive temperature trend that would balance the positive density tendency contribution from the denser air lifted upward by the pressure level rise.

In the second example we relax the assumption that $\overline{w}^*$ and density remain constant and instead allow their local tendencies in the z-frame (as is the case in the model simulations). But now we assume a special situation that the net upwelling diagnosed following the rising pressure levels remains constant. In such a situation, we would obtain a strict compensation between the negative z term and the positive ρ and $\overline{w}^*$ terms. As the pressure level moves systematically upwards, in the algorithm of the method this rise results in sampling of regions with climatologically smaller mass transport due to the exponential decrease of the mass flux with height, as quantified by the z term. At the same time, the upward shift of the pressure surfaces projects to the density increase and circulation changes at a fixed altitude (in sign and magnitude dependent on the $\overline{w}^*$ vertical distribution). In this limiting case, the interpretation of the $\overline{w}^*$ accelerating tendency would be that it is induced by the upward pressure level shift and requires that $\overline{w}^*$ decreases with height, which is the case in the tropical lower stratosphere.

In the third example, we discuss how the trends would be interpreted for the limiting case discussed by Oberländer-Hayn et al. (2016), if the circulation were fixed on isentropes rising at a greater pace than the pressure levels. Following a pressure level, the net upwelling trend (left hand side of Equation 4) would be positive because the pressure levels are moving downward relative to isentropes. How would this trend be interpreted by the decomposition method in the z-frame? The z term will be unchanged (negative) from the preceding examples,

because it is determined by the rise of pressure levels. However, the $\overline{w}^*$ term would show a much stronger positive trend. A slightly more complicated situation would emerge for the density trend, because the temperature effects would become at least comparable to the effect of rising pressure levels. But for the stable stratospheric stratification this should result in an even stronger positive ρ term tendency.

We note, that in the process of deriving the decomposition (Equation 4), we assume that the center of the upwelling region is shifting only negligibly in the meridional direction compared to the width of the upwelling region. This is well justified for the annual mean upwelling in the stratosphere, where the core of the upwelling region is located around the equator (e.g., see Figure 4 in Stiller et al., 2017). Under more general instances, relative meridional coordinates following the center of the upwelling region would have to be used at this stage and also for further partitioning to separate the effect of a net meridional shift of the upwelling region.

The omission of higher order of δt terms in (Equation 4), is well justified for the annual mean upwelling changes and the levels analyzed in this study. After comparing the net upwelling (left-hand side of Equation 4) computed directly from the data with its reconstruction from the sum of the right-hand side terms (discretization of the method is detailed in the Text S2 in Supporting Information S1), we see that the decomposition is highly accurate. For example, the correlation between the two time series of a directly computed and reconstructed net upwelling across the tropopause yields $R = 0.99$ when computed from ERA5 (Hersbach et al., 2020, see next section) annual mean data, and $R = 1.0$ for the upwelling across the two isobars.

2.1. Data

We analyze annual mean data from the Coupled Model Intercomparison project Phase 6 (CMIP6) simulations. Specifically, for the recent past we use the Atmospheric Model Intercomparison Project (AMIP) CMIP6 simulations and SSP370 (Eyring et al., 2016) simulations for future climate projections. CMIP6 models that have all the necessary outputs required for the proposed analysis (temperature, geopotential height, $\overline{v}^*$, $\overline{w}^*$, and the tropopause height) are CESM2 (Danabasoglu et al., 2020), CESM2-WACCM (Danabasoglu et al., 2020), MRI-ESM2-0 (Yukimoto et al., 2019) for both AMIP and SSP370 and UKESM1-0-LL (Sellar et al., 2020) only for SSP370. For each model the maximum number of available realizations was used. More detailed information on the individual models is given in Table S1 in Supporting Information S1. Along with the models, we used data from the three widely used reanalyses: ERA5 (Hersbach et al., 2020), JRA55 (Kobayashi et al., 2015), and MERRA2 (Gelaro et al., 2017) to derive observational constraints on upwelling changes in AMIP simulations.

2.2. Statistical Analysis

We adopt the Dynamical Linear Modeling (DLM) regression from Alsing (2019). While Multiple Linear Regression has been considered a standard approach to assess long-term trends of atmospheric time series with a complex evolution, for example, prescribing an explanatory variable for the trend estimation and its aliasing with other regressors (Kuchar et al., 2017), DLM represents a regression framework with the ability of regression coefficients to evolve in time. This allows DLM to assess the non-linear background trend which corresponds better with non-stationary processes in the atmosphere (Laine et al., 2014). For these reasons, DLM has been recently used to estimate trends in ozone in model outputs (Ball et al., 2018; Karagodin-Doyennel et al., 2022) and observational records (Bognar et al., 2022; Laine et al., 2014; Maillard Barras et al., 2022) quite extensively.

We use the Markov chain Monte Carlo method to infer the posterior distributions of the background level, autoregressive coefficient (AR1) and regression coefficient of the El Niño–Southern Oscillation (ENSO) variability. This method represents Bayesian DLM estimation of model states, parameters and their uncertainties. We input the ensemble mean and spread of individual models into the DLM regression to capture their forced response and model their time-dependent uncertainty. To illustrate the spread/uncertainties across reanalyses and model ensembles, we visualize the probability density functions of the individual contributions to BDC change in violin plots throughout the manuscript. When we refer to a multi-reanalysis mean (MRM), we average time series from MERRA2, JRA55 and ERA5 together, and we input MRM and its spread into DLM consequently. Thus, the reanalysis spread propagates into the uncertainties of our trend results.

We use here the same DLM model as Ball et al. (2018) but without a seasonal cycle. We also allow higher variance of the local trend resulting in higher variability of the background trend on shorter timescales since we use ENSO as the only regressor. For the ENSO variability in future CMIP6 simulations, we use the first principal

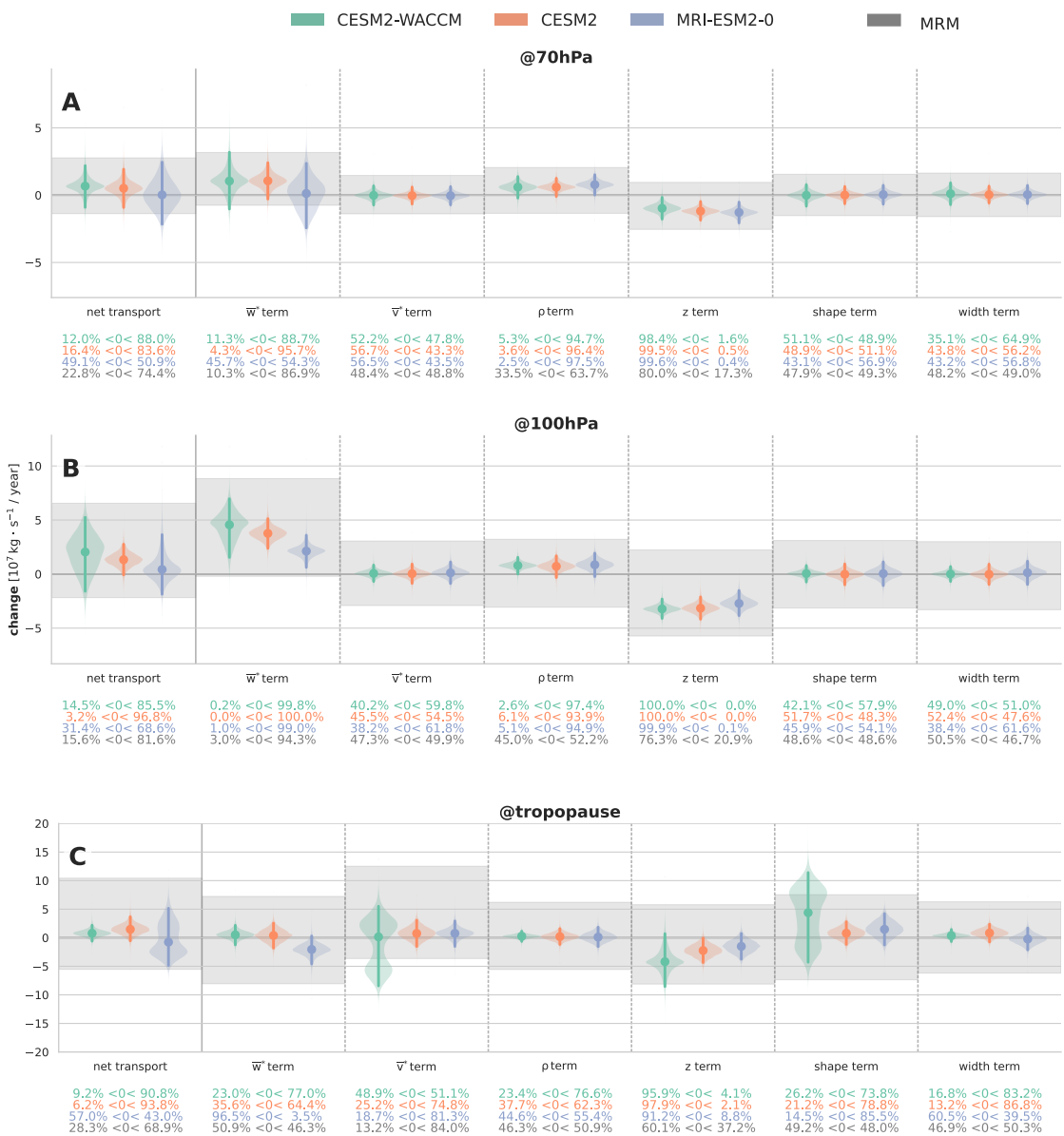

Figure 2. Interannual change of the net upwelling and the contributing terms at 70 hPa (top), 100 hPa (middle) and the tropopause (bottom) for the period 1979–2015. The dots in the individual violin plots depict the position of the median and vertical lines represent the 95% credible interval (also called the highest density interval–HDI). The HDI of the multi-reanalysis mean (MRM: ERA5, JRA55 and MERRA2; see also Figure S2 in Supporting Information S1 for their comparison) is represented by the gray band. Note that MRM refers to averaged reanalysis time series not to averaged individual distributions. The colored numbers at the bottom denote the percentage of relative occurrence of negative or positive year-to-year upwelling changes.

component of the detrended SST anomalies in the tropical belt, 20°S and 20°N (e.g., Berner et al., 2020) from each model. For the ENSO variability in the AMIP simulations, we use the observed ENSO index. Variation of the BDC and its proxies are explained mostly by internal variability in the tropics (Iglesias-Suarez et al., 2021). We tested multiple configurations, for example, including QBO regressors, but the results confirm a large dependency of transport terms on ENSO.

3. Results

Here we apply the method described in Section 2 to the set of available CMIP6 AMIP ensemble simulations and compare the upwelling changes with the multi-reanalysis mean (MRM). In Figure 2 we show the resulting

posterior distribution of the interannunal changes (trend) in the net upwelling over 1979–2014, together with the decomposition to contributions from the individual mechanisms. Discussing the net upwelling changes for individual models first, MRI at TPP shows a large spread of the net upwelling changes with a double peak structure, more skewed toward negative values. At 100 hPa and especially at 70 hPa, MRI continues to show a large spread of the changes with almost no robust systematic change. From the same model family, CESM2 and CESM2-WACCM simulate increasing net upwelling across all three studied levels with the best agreement at 70 hPa, but they also slightly disagree regarding the magnitude and spread of the changes at TPP and 100 hPa. This is documented also by the occurrence frequency of year-to-year upwelling changes (positive or negative, see individual numbers below the plots in Figure 2). Generally, there is a good agreement between the models in the net upwelling across the pressure levels and only at TPP the models do not fully agree on the sign of the change. Constraining the model net upwelling changes with the MRM confidence interval, only a tiny portion of the negative upwelling changes at TPP and a slightly larger portion at 70 hPa simulated by MRI falls outside the MRM interval.

Applying the decomposition methodology to the net upwelling trend at 70 hPa, the largest variations are attributed to the term connected with the vertical component of the residual mean circulation ($\overline{w}^*$) with almost equally strong systematic contributions from the density and upward shift terms. Altogether, the high degree of compensation points toward the importance of the upward shift of the 70 hPa isobar for changes reconstructed in the z-coordinate. Specifically for MRI, the pronounced upward shift of the 70 hPa isobar that projects strongly to the z and ρ terms, does not project to the local accelerations of $\overline{w}^*$, suggesting a slightly different climatological vertical structure of $\overline{w}^*$ in MRI in this region. The other kinematic factors ($\overline{v}^*$, width and shape terms) show a negligible systematic influence on the net upwelling trend at 70 hPa except for CESM2-WACCM showing a small positive systematic contribution from widening of the upwelling region.

Decomposing the net upwelling at the 100 hPa level, the contributions from all the terms for all models fall within the MRM confidence interval. For MRI, in contrast to the decomposition at 70 hPa, the $\overline{w}^*$ is clearly positive with much smaller spread, still the $\overline{w}^*$ term trend is significantly smaller than for CESM2 and CESM2-WACCM. The three models show similar systematic positive contributions from the density term, although the vertical shift term is smaller in MRI, which is connected with a slightly weaker temperature trend at 100 hPa for this model (see Figure S1 in Supporting Information S1). The resulting uncertain net upwelling trend for MRI at 100 hPa is skewed toward positive values partly due to the mainly positive contributions from the $\overline{v}^*$ and the width terms.

At TPP (the bottom row of Figure 2), which is characterized by a more complex geometry, the net upwelling changes result from competing effects between the different mechanisms. Here all the terms contribute with a very similar magnitude, except the density term, which is negligible in this region. The largest and predominantly positive contributions to the net upwelling stem from the term connected with the accelerating meridional component of the residual mean circulation ($\overline{v}^*$) and the tropopause shape term. These two mechanisms are connected, because, as the tropopause gets more inclined, the efficiency of the accelerating $\overline{v}^*$ for cross-tropopause transport further increases. For CESM2 and CESM2-WACCM we find also a small, but systematic positive contribution from the width term. The two related models differ at TPP strongly in the shape and vertical shift term and also in the spread of the ($\overline{v}^*$) term. Interestingly, the large spread of changes in these three terms in CESM2-WACCM (also exceeding the MRM confidence interval) largely cancels out and the resulting positive net upwelling trend is only slightly smaller and less significant for CESM2-WACCM than for CESM2. The situation is different for MRI, where we see a strong negative contribution from the $\overline{w}^*$ term. This term is not compensated, but out of phase with the terms contributing to the positive change resulting in a bimodal distribution of the net upwelling with a large spread, skewed toward negative values. Note, however, that it completely lies inside the MRM confidence interval.

In Figure 2 it is shown that the 95% credible interval of MRM in the majority of cases cannot constrain the differences between the models. This is attributable to the surprisingly large differences between the individual reanalyses in the net upwelling and the contributions from individual mechanisms. In Figure 3 we combine the analysis of the interannual change distribution with the scatter plot to illustrate the relationship between the trend in net upwelling and the contributing terms. For clarity of presentation, we show in Figure 3 only the results for the ($\overline{w}^*$), vertical shift and width terms. For the results of the full decomposition for individual reanalyses we refer the interested reader to the Figure S2 in Supporting Information S1, where the contribution of all terms is visualized using the violin plots of interannual change distribution.

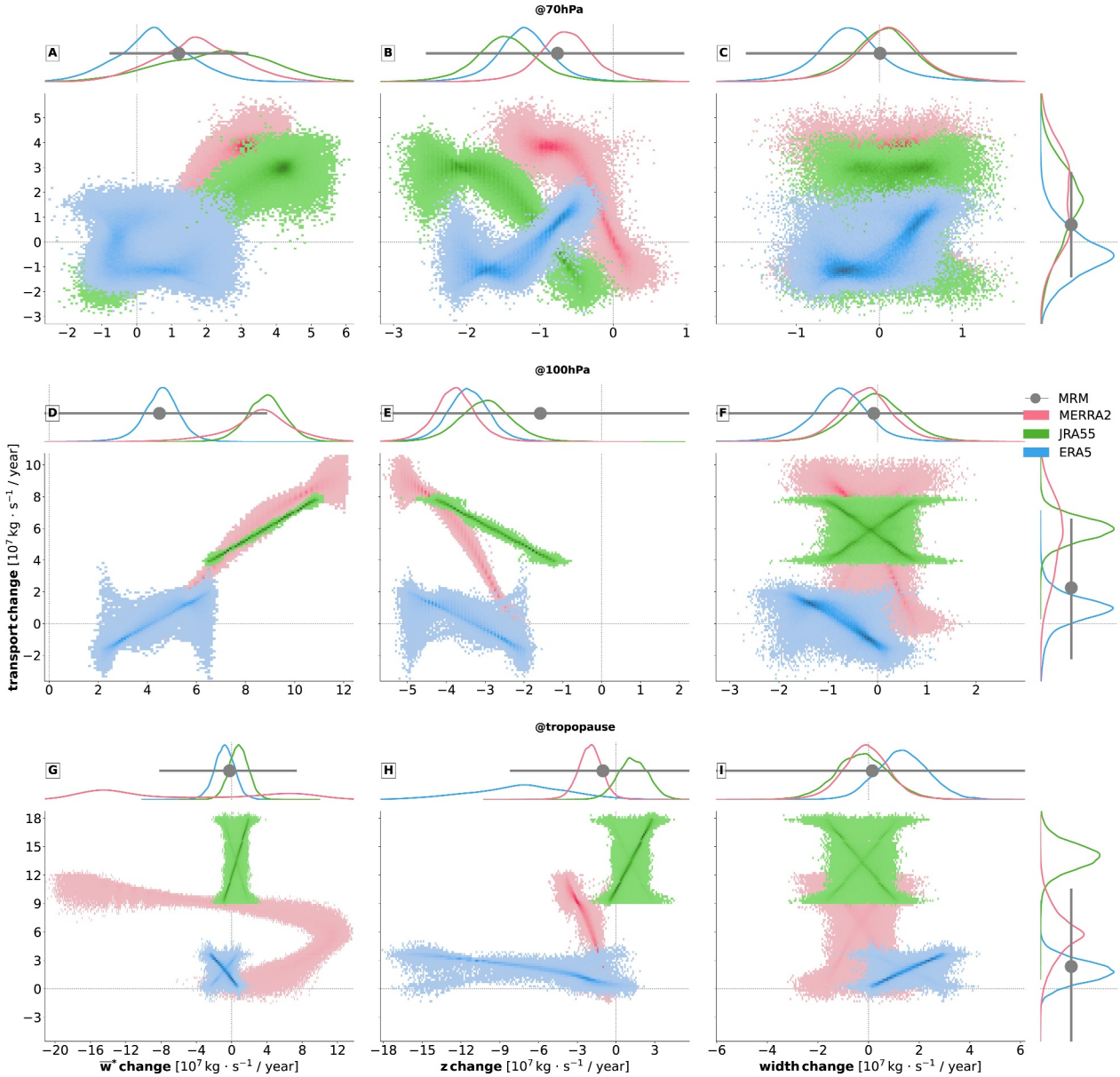

Figure 3. Interannual change (distribution plots) and trend (scatter plots) of the net upwelling in relationship with $\overline{w}^*$, z and width terms at 70 hPa (top), 100 hPa (middle) and the tropopause (bottom) for the period 1980–2015. Individual reanalyses are shown with different colors. Note that the scales of both axes differ for each plot. Relationships between trend terms shown as scatter points are transformed by quantile normalization (for visualization purposes). Distributions of interannual changes (slopes) are provided as side plots and bear similar information as the violins in Figure 2. The HDI of the multi-reanalysis mean (MRM) is represented by the gray point with error line. Note that MRM refers to averaged reanalysis time series not to averaged individual distributions.

Figure 3 (distribution plots at the right-hand side boundary of the figure) reveals that all three reanalyses agree on the systematically increasing net upwelling at the tropopause and 100 hPa and also at 70 hPa with the exception of ERA5. At 70 hPa, the net upwelling change in the ERA5 reanalysis has a large uncertainty but points toward a slight systematic weakening. At the tropopause and 100 hPa, the net upwelling changes in ERA5 are predominantly positive, but also weaker compared to the other two reanalyses. For MERRA2, an interesting aspect of the net upwelling changes is that at all analyzed levels it shows a large spread of the changes resulting in a much broader distribution of the interannual changes compared to JRA55 and ERA5, particularly at 100 hPa.

The decomposition reveals several interesting aspects behind the differences of the net upwelling changes between the reanalyses. We start discussing the least complicated width term, for which we find at each analyzed

level a difference between ERA5 and the other two reanalyses. At 70 hPa and 100 hPa (panels C and F), the width term contribution is systematically negative, as the upwelling region narrows down in ERA5. But, at TPP (Figure 3i) the upwelling region widens in ERA5. Also, note that in ERA5 the relationship between the width term and the net upwelling changes is different at TPP and 70 hPa (wider upwelling region resulting in increasing net upwelling) and at 100 hPa (narrower upwelling region–increasing net upwelling).

ERA5 shows differences compared to the other two reanalyses also in a much stronger upward shift contribution at TPP (panel H) and in a different relationship at 70 hPa between the net upwelling trend and vertical shift (panel B) and $\overline{w}^*$ term changes (panel A). For ERA5 there is no clear relationship between the $\overline{w}^*$ term and the net upwelling changes detectable from the scatter plot. In contrast, we see strong positive correlations in JRA55 and MERRA2. In ERA5, across all levels, the $\overline{w}^*$ term contributes much less to the net upwelling change than in the other two reanalyses, although the vertical shift terms are comparable between reanalyses.

MERRA2 and JRA55 agree remarkably well in the decomposition except at TPP, where we identify in JRA55 positive contributions from the vertical shift term (panel H) and in MERRA2 a pronounced double peak structure and nonlinear relationship with the net upwelling change for the $\overline{w}^*$ term (see Figure 3g). Nevertheless, for the upwelling across TPP it has to be noted that the strongest contribution comes from the $\overline{v}^*$ term, where MERRA2 and JRA55 agree remarkably well (see Figure S2 in Supporting Information S1).

4. Conclusions

In this study, we have derived and applied a novel methodology that allows a more nuanced view into the advective BDC changes by decomposing the net upwelling change following a pressure surface or the tropopause into contributions diagnosed in the geometric vertical coordinate from accelerating advection by the residual mean circulation, local density changes, and changes in the vertical and horizontal structure of the atmosphere in response to climate change. The method can be applied to any iso-surface such as isentropic, pressure or theta levels, or the tropopause. A combination of the decomposition method and dynamic linear modeling helped to reveal completely different (non-linear) links between individual mechanisms and the net upwelling changes in the model and reanalysis data.

We demonstrate the performance of the decomposition method on an ensemble of CMIP6 simulations and on a set of reanalyses. The results reveal that when viewed in the z-frame, the changes in the net tropical upwelling are composed from a variable mixture of acceleration of the vertical advection and vertical shifts of the circulation influencing also the density of air and, as a novel aspect, we show that the horizontal structure changes can be an important component contributing to the net-upwelling change as well. The relative roles of these mechanisms differ between the levels. In particular, the horizontal structure changes are important mostly at the tropopause, influencing the widening of the upwelling region and the contribution from the meridional mass flux component.

For the models, we have found an excellent agreement for the upwelling trends across 70 and 100 hPa. The agreement is only slightly worse for the net upwelling trend across the tropopause. The decomposition reveals that the good agreement across all levels is a result of compensation between the effects of different mechanisms identified in the z-frame. The agreement between the models on the importance of the individual terms of the decomposition is also remarkably good for the upwelling across the pressure levels, however, across the tropopause there are pronounced differences between the models regarding the role of the meridional circulation and the tropopause shape changes. Similar conclusions hold also for projections of future net upwelling changes and their decomposition (Figure S3 in Supporting Information S1 and related discussion in Text S3 in Supporting Information S1).

As an important result of our study, we have shown that current reanalyses cannot sufficiently help to constrain the model differences in the net tropical upwelling change or in the individual contributing mechanisms revealed in the z-frame. The MRM confidence intervals in most cases are much larger than differences across the models. This means that the agreement between individual reanalyses in both the net upwelling across analyzed levels and the decomposition is weaker than between the models. For instance, ERA5 points to unambiguous systematic contributions of the upwelling region width changes at all studied levels, which is not mirrored in the MERRA2 and JRA55 reanalyses. A possible explanation is that the width term is particularly sensitive to the horizontal resolution due to the impact on accuracy of the turn-around latitude detection and/or due to the improved resolution of meso-scale processes (Hoffmann & Spang, 2022). Especially, gravity waves present a considerable

forcing at the edges of the tropical upwelling region in the lower stratosphere. In the near future, the inclusion of upcoming reanalyses such as JRA3Q, which is closer to ERA5 regarding the horizontal and vertical resolution, can shed some light on this issue.

Additionally, we have found pronounced differences between the reanalyses concerning the interannual variability and trend of the vertical component of the residual mean circulation and also in the relationship between the vertical structure and the net upwelling changes. This can be due to different data assimilation methodologies or representation of ozone-climate interactions (Abalos et al., 2019), although we have verified that the reanalyses agree well on the temperature evolution at the diagnosed levels (Figure S2 in Supporting Information S1).

Correctly simulating all the aspects of the advective BDC spatio-temporal variability and long-term trends is a challenging task for ESMs and reanalyses, as it requires representing all the involved mechanisms accurately (in terms of timing, location, strength, and amplitude). For instance for studies of tracer trends or age-of-air it makes a difference whether the same net upwelling trend on pressure surface is caused by locally accelerating circulation velocities, widening of the upwelling region, or by the upward shift of the circulation. The accuracy of the simulated composition changes is critical for a quantitative understanding of the climate change influence on the middle atmosphere.

Besides being a great tool for comparing the skill in simulating the co-occurring BDC and atmospheric structure changes across the data sets, a large potential benefit of the presented method is that it explicitly highlights novel constraints, to date unconsidered in the BDC research. Unlike the changes in the residual mean circulation alone, the horizontal structure, density (temperature) and vertical shift changes can be directly observable (either from ground or space) and, subject to availability of sufficiently long and homogeneous observational time series, can guide improved matching of simulated BDC trends with observations. We therefore encourage future research and planning of observational capabilities in this direction.

Data Availability Statement

CMIP6 data can be downloaded from https://esgf-node.llnl.gov/search/cmip6/. ERA5 data are available at Hersbach et al. (2023). JRA55 and MERRA2 zonal mean data was obtained from S-RIP project stored at CEDA archive at Martineau and Wright (2017). The tropopause data for JRA55 can be obtained by contacting Dr. Sean Davis and Dr. Susann Tegtmeier and for ERA5 and MERRA2 tropopause characteristics by Dr. Lars Hoffmann. Transport and decomposition time series are stored at Zenodo (Zajíček, 2023). All codes are available on request to the corresponding author.

Acknowledgments
We would like to thank the reviewers and the editor for helping us to substantially improve the manuscript during the review process, Zuzana Procházková for discussions on the analytical derivation of the method, Sean Davis and Susann Tegtmeier for the JRA55 tropopauses and Lars Hoffmann for the ERA5 and MERRA2 tropopauses. Funding: Czech Science Foundation JUNIOR-STAR Grant 23-04921M; Czech Science Foundation Grant 21-03295S; Charles University, project GA UK No. 456622. Charles University Research Centre program No. UNCE/24/SCI/005. AK and HR acknowledge support by the University of Natural Resources and Life Sciences, Vienna. This research was also partly supported by the International Space Science Institute (ISSI) in Bern, through ISSI International Team project 544 (Impacts of Climate Change on the Middle and Upper Atmosphere and Atmospheric Drag of Space Objects).

References

Abalos, M., Calvo, N., Benito, S., Garny, H., Hardiman, S., Lin, P., et al. (2021). The Brewer–Dobson circulation in CMIP6. *Atmospheric Chemistry and Physics*, *21*(17), 13571–13591. https://doi.org/10.5194/acp-21-13571-2021

Abalos, M., Polvani, L., Calvo, N., Kinnison, D., Ploeger, F., Randel, W., & Solomon, S. (2019). New insights on the impact of ozone-depleting substances on the Brewer-Dobson circulation. *Journal of Geophysical Research: Atmospheres*, *124*(5), 2435–2451. https://doi.org/10.1029/2018JD029301

Alsing, J. (2019). DLMMC: Dynamical linear model regression for atmospheric time-series analysis. *Journal of Open Source Software*, *4*(37), 1157. https://doi.org/10.21105/joss.01157

Andrews, D. G., Holton, J. R., & Leovy, C. B. (1987). *Middle atmosphere dynamics*. Academic Press.

Ball, W. T., Alsing, J., Mortlock, D. J., Staehelin, J., Haigh, J. D., Peter, T., et al. (2018). Evidence for a continuous decline in lower stratospheric ozone offsetting ozone layer recovery. *Atmospheric Chemistry and Physics*, *18*(2), 1379–1394. https://doi.org/10.5194/acp-18-1379-2018

Berner, J., Christensen, H. M., & Sardeshmukh, P. D. (2020). Does ENSO regularity increase in a warming climate? *Journal of Climate*, *33*(4), 1247–1259. https://doi.org/10.1175/JCLI-D-19-0545.1

Bognar, K., Tegtmeier, S., Bourassa, A., Roth, C., Warnock, T., Zawada, D., & Degenstein, D. (2022). Stratospheric ozone trends for 1984–2021 in the SAGE II–OSIRIS–SAGE III/ISS composite dataset. *Atmospheric Chemistry and Physics*, *22*(14), 9553–9569. https://doi.org/10.5194/acp-22-9553-2022

Butchart, N. (2014). The Brewer-Dobson circulation. *Reviews of Geophysics*, *52*(2), 157–184. https://doi.org/10.1002/2013RG000448

Butchart, N., Cionni, I., Eyring, V., Shepherd, T. G., Waugh, D. W., Akiyoshi, H., et al. (2010). Chemistry–climate model simulations of twenty-first century stratospheric climate and circulation changes. *Journal of Climate*, *23*(20), 5349–5374. https://doi.org/10.1175/2010JCLI3404.1

Danabasoglu, G., Lamarque, J.-F., Bacmeister, J., Bailey, D. A., DuVivier, A. K., Edwards, J., et al. (2020). The community earth system model version 2 (CESM2). *Journal of Advances in Modeling Earth Systems*, *12*(2), e2019MS001916. https://doi.org/10.1029/2019MS001916

Davis, S. M., Davis, N., Portmann, R. W., Ray, E., & Rosenlof, K. (2023). The role of tropical upwelling in explaining discrepancies between recent modeled and observed lower-stratospheric ozone trends. *Atmospheric Chemistry and Physics*, *23*(5), 3347–3361. https://doi.org/10.5194/acp-23-3347-2023

Eichinger, R., Dietmüller, S., Garny, H., Šácha, P., Birner, T., Bönisch, H., et al. (2019). The influence of mixing on the stratospheric age of air changes in the 21st century. *Atmospheric Chemistry and Physics*, *19*(2), 921–940. https://doi.org/10.5194/acp-19-921-2019

Eichinger, R., & Šácha, P. (2020). Overestimated acceleration of the advective Brewer-Dobson circulation due to stratospheric cooling. *Quarterly Journal of the Royal Meteorological Society*, *146*(733), 3850–3864. https://doi.org/10.1002/qj.3876

Eyring, V., Bony, S., Meehl, G. A., Senior, C. A., Stevens, B., Stouffer, R. J., & Taylor, K. E. (2016). Overview of the coupled model intercomparison project phase 6 (CMIP6) experimental design and organization. *Geoscientific Model Development*, *9*(5), 1937–1958. https://doi.org/10.5194/gmd-9-1937-2016

Fu, Q., & Lin, P. (2011). Poleward shift of subtropical jets inferred from satellite-observed lower-stratospheric temperatures. *Journal of Climate*, *24*(21), 5597–5603. https://doi.org/10.1175/JCLI-D-11-00027.1

Garcia, R. R., & Randel, W. J. (2008). Acceleration of the Brewer–Dobson circulation due to increases in greenhouse gases. *Journal of the Atmospheric Sciences*, *65*(8), 2731–2739. https://doi.org/10.1175/2008JAS2712.1

Gelaro, R., McCarty, W., Suárez, M. J., Todling, R., Molod, A., Takacs, L., et al. (2017). The modern-era retrospective analysis for research and applications, version 2 (MERRA-2). *Journal of Climate*, *30*(14), 5419–5454. https://doi.org/10.1175/JCLI-D-16-0758.1

Hardiman, S., Butchart, N., & Calvo, N. (2014). The morphology of the Brewer–Dobson circulation and its response to climate change in CMIP5 simulations. *Quarterly Journal of the Royal Meteorological Society*, *140*(683), 1958–1965. https://doi.org/10.1002/qj.2258

Hersbach, H., Bell, B., Berrisford, P., Biavati, G., Horányi, A., Muñoz Sabater, J., et al. (2023). ERA5 hourly data on pressure levels from 1940 to present [Dataset]. *Copernicus Climate Change Service (C3S) Climate Data Store (CDS)*. https://doi.org/10.24381/cds.bd0915c6

Hersbach, H., Bell, B., Berrisford, P., Hirahara, S., Horányi, A., Muñoz-Sabater, J., et al. (2020). The ERA5 global reanalysis. *Quarterly Journal of the Royal Meteorological Society*, *146*(730), 1999–2049. https://doi.org/10.1002/qj.3803

Hoffmann, L., & Spang, R. (2022). An assessment of tropopause characteristics of the ERA5 and era-interim meteorological reanalyses. *Atmospheric Chemistry and Physics*, *22*(6), 4019–4046. https://doi.org/10.5194/acp-22-4019-2022

Iglesias-Suarez, F., Wild, O., Kinnison, D. E., Garcia, R. R., Marsh, D. R., Lamarque, J.-F., et al. (2021). Tropical stratospheric circulation and ozone coupled to pacific multi-decadal variability. *Geophysical Research Letters*, *48*(11), e2020GL092162. https://doi.org/10.1029/2020GL092162

IPCC. (2022). In P. Shukla et al. (Eds.), *Climate change 2022: Mitigation of climate change. contribution of working group iii to the sixth assessment report of the intergovernmental panel on climate change*. Cambridge University Press. https://doi.org/10.1017/9781009157926

Karagodin-Doyennel, A., Rozanov, E., Sukhodolov, T., Egorova, T., Sedlacek, J., Ball, W., & Peter, T. (2022). The historical ozone trends simulated with the SOCOLV4 and their comparison with observations and reanalysis. *EGUsphere*, *2022*, 1–26. https://doi.org/10.5194/acp-22-15333-2022

Kobayashi, S., Ota, Y., Harada, Y., Ebita, A., Moriya, M., Onoda, H., et al. (2015). The JRA-55 reanalysis: General specifications and basic characteristics. *Journal of the Meteorological Society of Japan*, *93*(1), 5–48. https://doi.org/10.2151/jmsj.2015-001

Kuchar, A., Ball, W. T., Rozanov, E. V., Stenke, A., Revell, L., Miksovsky, J., et al. (2017). On the aliasing of the solar cycle in the lower stratospheric tropical temperature. *Journal of Geophysical Research: Atmospheres*, *122*(17), 9076–9093. https://doi.org/10.1002/2017JD026948

Laine, M., Latva-Pukkila, N., & Kyrölä, E. (2014). Analysing time-varying trends in stratospheric ozone time series using the state space approach. *Atmospheric Chemistry and Physics*, *14*(18), 9707–9725. https://doi.org/10.5194/acp-14-9707-2014

Maillard Barras, E., Haefele, A., Stübi, R., Jouberton, A., Schill, H., Petropavlovskikh, I., et al. (2022). Dynamical linear modeling estimates of long-term ozone trends from homogenized Dobson Umkehr profiles at Arosa/Davos, Switzerland. *Atmospheric Chemistry and Physics*, *22*(21), 14283–14302. https://doi.org/10.5194/acp-22-14283-2022

Martineau, P., & Wright, J. (2017). SPARC reanalysis intercomparison project (S-RIP): Zonal-mean global atmospheric reanalyses on pressure levels [Dataset]. *Centre for Environmental Data Analysis*. http://catalogue.ceda.ac.uk/uuid/dafbd838e4cc4c68a5ccdd90690ea57f

Maycock, A. C., Randel, W. J., Steiner, A. K., Karpechko, A. Y., Christy, J., Saunders, R., et al. (2018). Revisiting the mystery of recent stratospheric temperature trends. *Geophysical Research Letters*, *45*(18), 9919–9933. https://doi.org/10.1029/2018GL078035

Muthers, S., Kuchar, A., Stenke, A., Schmitt, J., Anet, J. G., Raible, C. C., & Stocker, T. F. (2016). Stratospheric age of air variations between 1600 and 2100. *Geophysical Research Letters*, *43*(10), 5409–5418. https://doi.org/10.1002/2016GL068734

Oberländer-Hayn, S., Gerber, E. P., Abalichin, J., Akiyoshi, H., Kerschbaumer, A., Kubin, A., et al. (2016). Is the Brewer-Dobson circulation increasing or moving upward? *Geophysical Research Letters*, *43*(4), 1772–1779. https://doi.org/10.1002/2015GL067545

Ortland, D., & Alexander, M. (2014). The residual-mean circulation in the tropical tropopause layer driven by tropical waves. *Journal of the Atmospheric Sciences*, *71*(4), 1305–1322. https://doi.org/10.1175/JAS-D-13-0100.1

Pisoft, P., Sacha, P., Polvani, L. M., Añel, J. A., de la Torre, L., Eichinger, R., et al. (2021). Stratospheric contraction caused by increasing greenhouse gases. *Environmental Research Letters*, *16*(6), 064038. https://doi.org/10.1088/1748-9326/abfe2b

Plumb, R. A. (2002). Stratospheric transport. *Journal of the Meteorological Society of Japan. Ser. II*, *80*(4B), 793–809. https://doi.org/10.2151/jmsj.80.793

Polvani, L. M., Abalos, M., Garcia, R., Kinnison, D., & Randel, W. J. (2018). Significant weakening of Brewer-Dobson circulation trends over the 21st century as a consequence of the Montreal protocol. *Geophysical Research Letters*, *45*(1), 401–409. https://doi.org/10.1002/2017GL075345

Šácha, P., Eichinger, R., Garny, H., Pisoft, P., Dietmüller, S., de la Torre Ramos, L., et al. (2019). Extratropical age of air trends and causative factors in climate projection simulations. *Atmospheric Chemistry and Physics*, *19*(11), 7627–7647. https://doi.org/10.5194/acp-19-7627-2019

Santer, B. D., Po-Chedley, S., Zhao, L., Zou, C.-Z., Fu, Q., Solomon, S., et al. (2023). Exceptional stratospheric contribution to human fingerprints on atmospheric temperature. *Proceedings of the National Academy of Sciences*, *120*(20), e2300758120. https://doi.org/10.1073/pnas.2300758120

Santer, B. D., Wehner, M. F., Wigley, T. M. L., Sausen, R., Meehl, G. A., Taylor, K. E., et al. (2003). Contributions of anthropogenic and natural forcing to recent tropopause height changes. *Science*, *301*(5632), 479–483. https://doi.org/10.1126/science.1084123

Scientific assessment of ozone depletion: Executive summary, 2022. (2022). p. 51. Retrieved from http://digitallibrary.un.org/record/4000934

Sellar, A. A., Walton, J., Jones, C. G., Wood, R., Abraham, N. L., Andrejczuk, M., et al. (2020). Implementation of U.K. earth system models for CMIP6. *Journal of Advances in Modeling Earth Systems*, *12*(4), e2019MS001946. https://doi.org/10.1029/2019MS001946

Shepherd, T., & McLandress, C. (2011). A robust mechanism for strengthening of the Brewer-Dobson circulation in response to climate change: Critical-layer control of subtropical wave breaking. *Journal of The Atmospheric Sciences*, *68*(4), 784–797. https://doi.org/10.1175/2010JAS3608.1

Solomon, S., Rosenlof, K. H., Portmann, R. W., Daniel, J. S., Davis, S. M., Sanford, T. J., & Plattner, G.-K. (2010). Contributions of stratospheric water vapor to decadal changes in the rate of global warming. *Science*, *327*(5970), 1219–1223. https://doi.org/10.1126/science.1182488

Staten, P., Grise, K., Davis, S., Karnauskas, K., Waugh, D., Maycock, A., et al. (2020). Tropical widening: From global variations to regional impacts. *Bulletin of the American Meteorological Society*, *101*(6), E897–E904. https://doi.org/10.1175/BAMS-D-19-0047.1

Stiller, G. P., Fierli, F., Ploeger, F., Cagnazzo, C., Funke, B., Haenel, F. J., et al. (2017). Shift of subtropical transport barriers explains observed hemispheric asymmetry of decadal trends of age of air. *Atmospheric Chemistry and Physics*, *17*(18), 11177–11192. https://doi.org/10.5194/acp-17-11177-2017

Vallis, G., Zurita-Gotor, P., Cairns, C., & Kidston, J. (2014). Response of the large-scale structure of the atmosphere to global warming. *Quarterly Journal of the Royal Meteorological Society*, *141*(690), 1479–1501. https://doi.org/10.1002/qj.2456

WMO. (2018). Scientific assessment of ozone depletion: 2018. *Global ozone research and monitoring project – Report no., 58, 588*.

Yukimoto, S., Kawai, H., Koshiro, T., Oshima, N., Yoshida, K., Urakawa, S., et al. (2019). The meteorological research institute earth system model version 2.0, MRI-ESM2.0: Description and basic evaluation of the physical component. *Journal of the Meteorological Society of Japan*, *97*(5), 931–965. https://doi.org/10.2151/jmsj.2019-051

Zajíček, R. (2023). Transport and decomposition time series [Dataset]. *Zenodo*. https://doi.org/10.5281/zenodo.8099089